Transition form factors: $\gamma^* + p \to \Delta(1232), \Delta(1600)$

Y. Lu,[1,*] C. Chen,[2,†] Z.-F. Cui,[1,‡] C. D. Roberts,[3,§] S. M. Schmidt,[4,‖] J. Segovia,[5,¶] and H.-S. Zong[1,6,**]

[1]*Department of Physics, Nanjing University, Nanjing, Jiangsu 210093, China*
[2]*Instituto de Física Teórica, Universidade Estadual Paulista, Rua Dr. Bento Teobaldo Ferraz, 271, 01140-070 São Paulo, São Paulo, Brazil*
[3]*Physics Division, Argonne National Laboratory, Lemont, Illinois 60439, USA*
[4]*Institute for Advanced Simulation, Forschungszentrum Jülich and JARA, D-52425 Jülich, Germany*
[5]*Departamento de Sistemas Físicos, Químicos y Naturales, Universidad Pablo de Olavide, E-41013 Sevilla, Spain*
[6]*Joint Center for Particle, Nuclear Physics and Cosmology, Nanjing, Jiangsu 210093, China*

(Received 11 April 2019; published 5 August 2019)

Electroproduction form factors describing the $\gamma^* p \to \Delta^+(1232)$, $\Delta^+(1600)$ transitions are computed using a fully dynamical diquark-quark approximation to the Poincaré-covariant three-body bound-state problem in relativistic quantum field theory. In this approach, the $\Delta(1600)$ is an analogue of the Roper resonance in the nucleon sector, appearing as the simplest radial excitation of the $\Delta(1232)$. Precise measurements of the $\gamma^* p \to \Delta^+(1232)$ transition already exist on $0 \leq Q^2 \lesssim 8$ GeV^2, and the calculated results compare favorably with the data outside the meson-cloud domain. The predictions for the $\gamma^* p \to \Delta^+(1600)$ magnetic dipole and electric quadrupole transition form factors are consistent with the empirical values at the real photon point, and extend to $Q^2 \approx 6 m_p^2$, enabling a meaningful direct comparison with experiment once analysis of existing data is completed. In both cases, the electric quadrupole form factor is particularly sensitive to deformation of the Δ-baryons. Interestingly, while the $\gamma^* p \to \Delta^+(1232)$ transition form factors are larger in magnitude than those for $\gamma^* p \to \Delta^+(1600)$ in some neighborhood of the real photon point, this ordering is reversed on $Q^2 \gtrsim 2 m_p^2$, suggesting that the $\gamma^* p \to \Delta^+(1600)$ transition is more localized in configuration space.

DOI: 10.1103/PhysRevD.100.034001

I. INTRODUCTION

The $\Delta(1232)$ family of baryons was the first of the resonances discovered in πN reactions [1–3]. With positive parity, isospin $I = \frac{3}{2}$, total spin $J = \frac{3}{2}$, and no net strangeness [4], the $\Delta^{+,0}$ members of this quadruplet have conventionally been viewed as the lightest isospin- and spin-flip excitations of the proton and neutron, respectively. Hence, since protons and neutrons (nucleons, N) are the basic elements of all nuclei, developing a detailed understanding of the Δ-baryons is of fundamental importance. Without this, hadron physics remains at a level akin to atomic physics based only on knowledge of the hydrogen atom's ground state.

Given that pions are a complex probe, there are advantages in exploiting the relative simplicity of virtual photons in order to chart Δ-resonance structure. Elastic form factors are empirically inaccessible because the $\Delta(1232)$-baryon lifetime is too small: $\tau_\Delta \sim 10^{-26} \tau_n$, where τ_n is the lifetime of a free neutron [4]. On the other hand, by exploiting intense, energetic electron beams at the Thomas Jefferson National Accelerator Facility, $\gamma^* p \to \Delta^+$ data are now available for $0 \leq Q^2 \lesssim 8$ GeV^2 [5–7]. These data have stimulated much theoretical analysis and speculation about, *inter alia*, the relevance of perturbative QCD (pQCD) to processes involving moderate momentum transfers [6–14]; hadron shape deformation [10–18]; and the role that resonance electroproduction experiments can play in exposing nonperturbative aspects of QCD, such as the nature of confinement and dynamical chiral symmetry breaking (DCSB) [7,19–21].

Just above the Δ-baryon level lies the nucleon's first positive-parity excitation, i.e., the Roper resonance, labeled $N(1440)1/2^+$. Discovered in 1963 [22–26], its characteristics were long the source of puzzlement because, e.g., constituent-quark potential models typically (and erroneously) produce a spectrum in which this excitation lies above the first negative-parity state $N(1535)1/2^-$ [27–29]. This has now changed following: acquisition and analysis of high-precision proton-target exclusive electroproduction

*luya@nju.edu.cn
†Chen.Chen@theo.physik.uni-giessen.de
Present address: Institut für Theoretische Physik, Justus-Liebig-Universität Gießen, 35392 Gießen, Germany.
‡phycui@nju.edu.cn
§cdroberts@anl.gov
‖s.schmidt@fz-juelich.de
¶jsegovia@upo.es
**zonghs@nju.edu.cn

data with single- and double-pion final states, on a large energy domain and with momentum transfers out to $Q^2 \approx 5$ GeV^2; development of a dynamical reaction theory capable of simultaneously describing all partial waves extracted from available, reliable data; and formulation and application of a Poincaré covariant approach to the continuum bound-state problem in relativistic quantum field theory. Today, it is widely accepted that the Roper is, at heart, the first radial excitation of the nucleon, consisting of a well-defined dressed-quark core that is augmented by a meson cloud, which both reduces the Roper's core mass by approximately 20% and contributes materially to the electroproduction form factors at low-Q^2 [30,31].

A similar pattern of energy levels is found in the spectrum of Δ-baryons. Namely, contradicting quark-model predictions [27–29], the first positive-parity excitation, $\Delta(1600)3/2^+$, lies below the negative parity $\Delta(1700)3/2^-$, with the splitting being approximately the same as that in the nucleon sector. This being the case and given the Roper-resonance example, it is likely that elucidating the nature of the $\Delta(1600)3/2^+$-baryon will require both (i) data on its electroproduction form factors which extends well beyond the meson-cloud domain and (ii) predictions for these form factors to compare with that data. The data exist [32,33] and can be analyzed with this aim understood. Herein, therefore, we provide the theoretical predictions.

Our treatment of the nucleon, $\Delta(1232)$- and $\Delta(1600)$-baryons, and the associated $\gamma N \to \Delta$ transitions is based on Refs. [13,34]. Capitalizing on this tight connection, herein we only sketch the elements of our calculation. (Isospin symmetry is assumed throughout.) Moreover, with nothing changed, our study delivers a unification of the $N \to \Delta(1232)$ and $N \to \Delta(1600)$ transitions.

Section II explains the quark-diquark approximation to the baryon problem in the context of a Poincaré-covariant Faddeev equation and discusses the solutions obtained for the $\Delta(1232)$-baryon and its first positive-parity excitation. The $\gamma^* p \to \Delta$ transition current and associated form factors are described in Sec. III. Section IV reports results for the $\gamma^* p \to \Delta(1232)$ transition, providing comparisons with data and other analyses. The $\gamma^* p \to \Delta(1600)$ transition form factors are discussed in Sec. V; Sec. VI describes their diquark and scatterer dissections; and Sec. VII provides a summary and offers perspectives.

II. BARYON WAVE FUNCTIONS

In relativistic quantum field theory, baryon structure is described by a Faddeev amplitude, obtained from a Poincaré-covariant Faddeev equation, which sums all possible quantum field theoretical exchanges and interactions that can take place between the three dressed quarks that characterize its valence-quark content. A dynamical prediction of Faddeev equation studies that employ realistic quark-quark interactions [35–38] is the appearance of

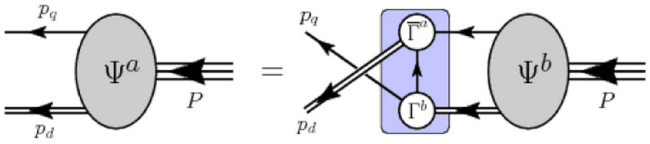

FIG. 1. Faddeev equation: a linear integral equation for the matrix-valued function Ψ, being the Faddeev amplitude for a baryon of total momentum $P = p_q + p_d$, which expresses the relative momentum correlation between the dressed quarks and nonpointlike diquarks within the baryon. The shaded rectangle demarcates the kernel of the Faddeev equation: *single line*, dressed-quark propagator; Γ, diquark correlation amplitude; and *double line*, diquark propagator.

nonpointlike quark + quark (diquark) correlations within baryons, whose characteristics are determined by DCSB [39–41]. Consequently, the baryon bound-state problem is transformed into solving the linear, homogeneous matrix equation in Fig. 1 [42–46]. Its key elements are the dressed-quark and -diquark propagators, and the diquark Bethe-Salpeter amplitudes.

Evidence supporting the presence of diquark correlations in baryons is accumulating, e.g., Refs. [11,13,14,21,34,47–57]. It should be emphasized that these correlations are fully dynamical and appear in a Faddeev kernel which requires their continual breakup and reformation. Consequently, they are vastly different from the static, pointlike diquarks introduced originally [58] in an attempt to solve the so-called "missing resonance" problem [5]. In fact, consistent with numerical simulations of lattice-regularized QCD [59], the spectrum of states produced by the Faddeev equation in Fig. 1 possesses a richness that cannot be explained by a two-body model.

To define the Faddeev equation in Fig. 1, we employ the elements specified in Refs. [13,34], which provide a successful description of the spectrum and structure of octet and decuplet baryons and their positive-parity excitations, and are part of a body of work that unifies a large array of hadron properties [31,60–62]. A key to these successes is DCSB, which produces a dressed-quark mass scale [36]: $M_D \simeq 0.4$ GeV, whose value underlies the natural size for mass-dimensioned quantities in the light-quark sector of the Standard Model.

With the inputs drawn from Refs. [13,34] (including light-quark scalar and axial-vector diquark masses $m_{0^+} = 0.79$ GeV and $m_{1^+} = 0.89$ GeV, respectively) one can readily construct the relevant Faddeev equation kernels and use *ARPACK* software [63] to obtain the mass and Faddeev amplitude of the $(I, J^P) = (1/2, 1/2^+)$ ground state (proton) and the two lightest $(I, J^P) = (3/2, 3/2^+)$ states, which we identify with the $\Delta(1232)$- and $\Delta(1600)$-baryons. The masses are (in GeV)

$$\begin{array}{ccc} m_p & m_{\Delta(1232)} & m_{\Delta(1600)} \\ 1.19 & 1.35 & 1.79 \end{array} . \tag{1}$$

These values correspond to the locations of the lowest-magnitude poles in the three-quark scattering problems in the given channels.

The residues associated with these poles are the Poincaré-covariant wave functions, $\chi(\ell^2, \ell \cdot P; P^2)$, where ℓ is the quark-diquark relative momentum. For every baryon considered herein, eight scalar functions are required to completely describe the system, each associated with a particular Dirac-matrix structure. For instance, the (amputated) Faddeev amplitude of any $(I, J^P) = (3/2, 3/2^+)$ baryon can be written in the following form:

$$\psi^{\Delta}(p_i, \alpha_i, \sigma_i) = \sum_{d \in \Delta} [\Gamma^d_{1^+\mu}(k; K)]^{\alpha_1 \alpha_2}_{\sigma_1 \sigma_2} \times \Delta^{1^+ d}_{\mu\nu}(K) [\varphi^{\Delta d}_{\nu\rho}(\ell; P) u_\rho(P)]^{\alpha_3}_{\sigma_3}, \quad (2)$$

where $(p_i, \sigma_i, \alpha_i)$ are the momentum, spin, and isospin labels of the quarks constituting the bound state; $P = p_1 + p_2 + p_3 = p_d + p_q$ is the total momentum of the baryon; $k = (p_1 - p_2)/2$, $K = p_1 + p_2 = p_d$, $\ell = (-K + 2p_3)/3$; d counts the diquarks participating in the baryon[1]; $\Gamma^d_{1^+\mu}$ and $\Delta^{1^+ d}_{\mu\nu}$ are, respectively, the associated correlation amplitude and propagator; $u_\rho(P)$ is a Rarita-Schwinger spinor (Ref. [13], Appendix B); and

$$\varphi^{\Delta d}_{\nu\rho}(\ell; P) = \sum_{k=1}^{8} \mathfrak{a}^d_{\Delta k}(\ell^2, \ell \cdot P) \mathcal{D}^k_{\nu\rho}(\ell; P), \quad (3a)$$

$$\mathcal{D}^k_{\nu\rho} = \mathcal{S}^k \delta_{\nu\rho}, \quad k = 1, 2, \quad (3b)$$

$$\mathcal{D}^k_{\nu\rho} = i\gamma_5 \mathcal{A}^{k-2}_\nu \ell^\perp_\rho, \quad k = 3, \ldots, 8, \quad (3c)$$

with

$$\begin{aligned} &\mathcal{S}^1 = \mathbf{I}_{\rm D}, \quad \mathcal{S}^2 = i\gamma \cdot \hat{\ell} - \hat{\ell} \cdot \hat{P} \mathbf{I}_{\rm D}, \\ &\mathcal{A}^1_\nu = \gamma \cdot \ell^\perp \hat{P}_\nu, \quad \mathcal{A}^2_\nu = -i\hat{P}_\nu \mathbf{I}_{\rm D}, \quad \mathcal{A}^3_\nu = \gamma \cdot \hat{\ell}^\perp \hat{\ell}^\perp_\nu, \\ &\mathcal{A}^4_\nu = i\hat{\ell}^\perp_\nu \mathbf{I}_{\rm D}, \quad \mathcal{A}^5_\nu = \gamma^\perp_\nu - \mathcal{A}^3_\nu, \quad \mathcal{A}^6_\nu = i\gamma^\perp_\nu \gamma \cdot \hat{\ell}^\perp - \mathcal{A}^4_\nu, \end{aligned} \quad (4)$$

$\hat{\ell}^2 = 1$, $\hat{P}^2 = -1$, $\ell^\perp = \hat{\ell}_\nu + \hat{\ell} \cdot \hat{P} \hat{P}_\nu$, $\gamma^\perp = \gamma_\nu + \gamma \cdot \hat{P} \hat{P}_\nu$. The (unamputated) Faddeev wave function, $\chi(\ell^2, \ell \cdot P; P^2)$, can be computed from the amplitude specified by Eqs. (2) and (3) simply by attaching the appropriate dressed-quark and diquark propagators. It may also be decomposed in the form of Eqs. (3). Naturally, the scalar functions are different, and we label them $\tilde{\mathfrak{a}}^d_{\Delta k}$.

In order to visualize the wave function solutions of the Faddeev equations, it is convenient to work with univariate Chebyshev projections of the scalar functions used to express them. Furthermore, as with mesons [64,65], one usually focuses on the zeroth functional moment of the given function ($u = \ell \cdot P / \sqrt{\ell^2 P^2}$),

$$\tilde{\mathfrak{a}}(\ell^2; P^2) = \frac{2}{\pi} \int_{-1}^{1} du \sqrt{1 - u^2} \tilde{\mathfrak{a}}(\ell^2, u; P^2), \quad (5)$$

because it is typically dominant in realistic solutions and hence expresses the largest amount of information.

The order-zero Chebyshev projections of the Faddeev wave function for the proton are plotted in Ref. [55], Fig. 4; and our calculation reproduces those results. Herein, therefore, in Fig. 2 we depict the projections for the ground-state Δ-baryon and its first positive-parity excitation. In all cases, we plot that combination of functions which has a well-defined value of quark-diquark orbital angular momentum in the baryon's rest frame. A key observation here is that, for the ground state, each projection is of a unique sign (positive or negative). On the other hand, with the exception of two D-wave components ($-\tilde{\mathfrak{a}}^{0,1}_6 + \tilde{\mathfrak{a}}^{0,1}_8$), all excited-state projections possess a single zero. As noted elsewhere [55,56,66,67], this pattern of behavior indicates that the positive-parity excitation may be interpreted as the simplest radial excitation of its ground-state partner.

Figure 2 also shows that the Δ-baryon ground-state and positive-parity excitation are primarily S-wave in character: the magnitudes of the curves in the top row are greater than those in the other rows. Naturally, we replicate the results of Ref. [34], viz. the ground-state mass is almost insensitive to non-S-wave components; and in the first positive-parity excitation, P-wave components generate a little repulsion, some attraction is provided by D-waves, and F-waves have no measurable impact. Evidently, too, some S-wave strength is shifted into P- and D-wave contributions within the positive-parity excitation [34,53,67]. Notwithstanding their smaller magnitudes, we will see that the higher partial waves have noticeable effects on electroproduction form factors.

Let us return to the masses in Eq. (1). Empirical values of these pole locations are [4] (in GeV): 0.939, $1.21 - i0.05$, $1.51 - i0.14$. (The physical Δ-baryons are unstable, and hence the associated pole has an imaginary part.) At first glance, these values appear unrelated to those in Eq. (1). However, deeper consideration reveals [68,69] that the kernel in Fig. 1 has an intrinsic weakness: resonant contributions, viz. meson-baryon final-state interactions (MB FSIs), are omitted. It is such effects which are resummed in dynamical coupled channel models, generating the widths and thereby transforming bare baryons into the observed states [70,71]. Our Faddeev equation should therefore be understood as producing the dressed-quark core of the bound state, not the completely dressed object.

Clothing the nucleon's dressed-quark core by including resonant contributions to the kernel produces a physical

[1]In Δ^+-baryons, the sum ranges over isovector-pseudovector $\{uu\}$, $\{ud\}$ correlations; and in Δ^0-baryons, $\{ud\}$ and $\{dd\}$. Assuming isospin symmetry, as we do throughout, the correlation amplitudes and propagators are identical for all these diquarks.

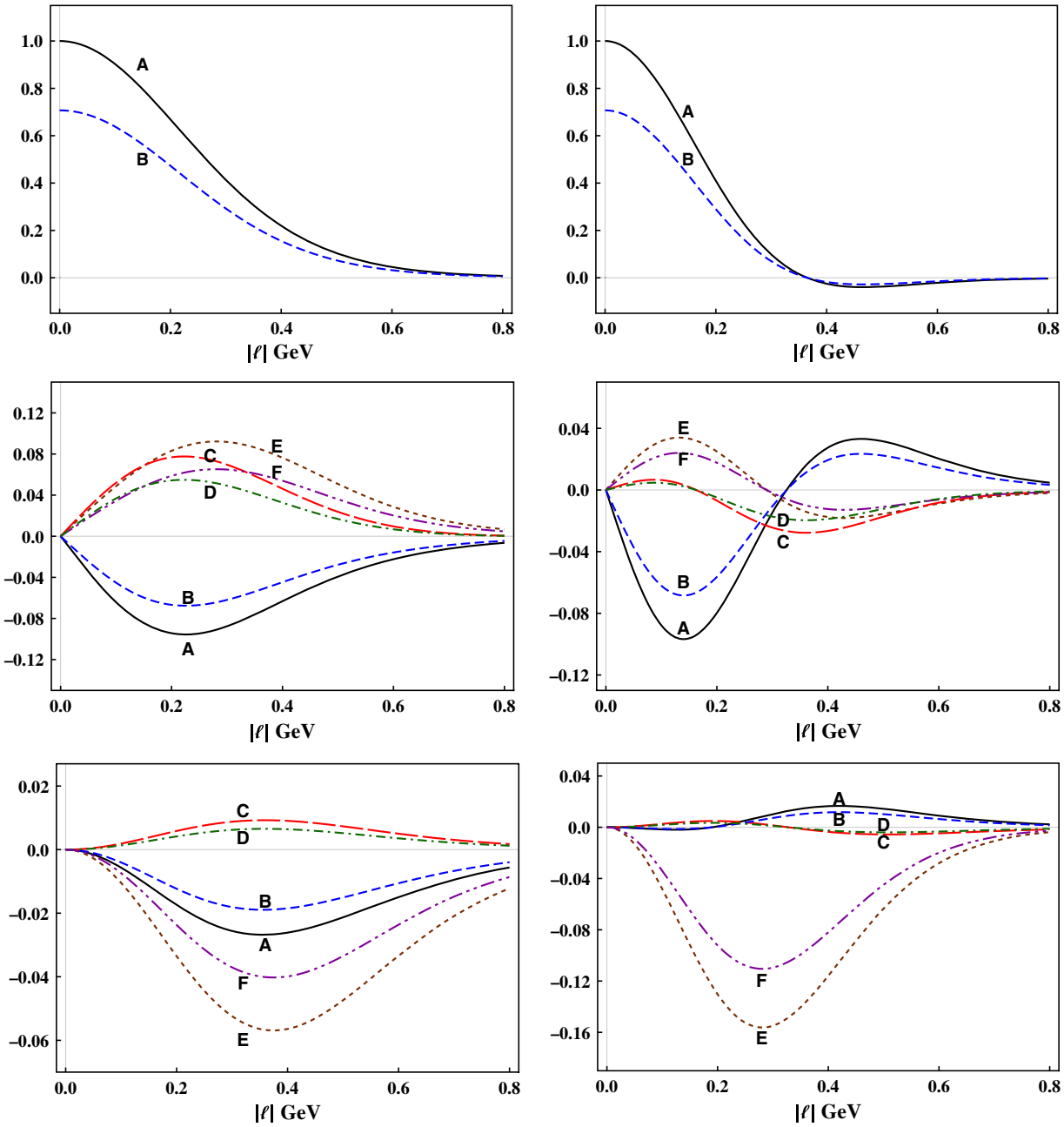

FIG. 2. Faddeev wave functions of Δ^+ baryons, zeroth Chebyshev-moment projections, Eq. (5): *left panels*—ground state; and *right panels*—first positive-parity excitation. Superscripts: "0" labels the pseudovector ($I = 1$, $I_z = 0$) $\{ud\}$-diquark; and "1" labels the pseudovector ($I = 1$, $I_z = 1$) $\{uu\}$-diquark. In the isospin-symmetry limit, the associated solution functions satisfy $\mathfrak{a}_k^0 = \sqrt{2}\mathfrak{a}_k^1$, $k = 1, \ldots, 8$. *S-wave*: top row. Legend. "A" $\to \tilde{\mathfrak{a}}_1^0 + (-\tilde{\mathfrak{a}}_6^0 + \tilde{\mathfrak{a}}_8^0)/3$; and "B" $\to \tilde{\mathfrak{a}}_1^1 + (-\tilde{\mathfrak{a}}_6^1 + \tilde{\mathfrak{a}}_8^1)/3$. *P-wave*: middle row. Legend. "A" $\to \tilde{\mathfrak{a}}_4^0$; "B" $\to \tilde{\mathfrak{a}}_4^1$; "C" $\to (2\tilde{\mathfrak{a}}_2^0 - \tilde{\mathfrak{a}}_5^0 - 2\tilde{\mathfrak{a}}_7^0)/3$; "D" $\to (2\tilde{\mathfrak{a}}_2^1 - \tilde{\mathfrak{a}}_5^1 - 2\tilde{\mathfrak{a}}_7^1)/3$; "E" $\to \tilde{\mathfrak{a}}_2^0 - (\tilde{\mathfrak{a}}_5^0 - \tilde{\mathfrak{a}}_7^0)/5$; and "F" $\to \tilde{\mathfrak{a}}_2^1 - (\tilde{\mathfrak{a}}_5^1 - \tilde{\mathfrak{a}}_7^1)/5$. *D-wave*: bottom row. Legend. "A" $\to \tilde{\mathfrak{a}}_3^0$; "B" $\to \tilde{\mathfrak{a}}_3^1$; "C" $\to -(\tilde{\mathfrak{a}}_6^0 + 2\tilde{\mathfrak{a}}_8^0)/3$; "D" $\to -(\tilde{\mathfrak{a}}_6^1 + 2\tilde{\mathfrak{a}}_8^1)/3$; "E" $\to -\tilde{\mathfrak{a}}_6^0 + \tilde{\mathfrak{a}}_8^0$; and "F" $\to -\tilde{\mathfrak{a}}_6^1 + \tilde{\mathfrak{a}}_8^1$. *F*-wave components are negligible for all decuplet baryons [34].

nucleon whose mass is ≈0.2 GeV lower than that of the core [72,73]. Similarly, MB FSIs reduce the $\Delta(1232)$-baryon's core mass by ≈0.16 GeV [74–76] and the Roper resonance's core mass by 0.3 GeV [76]. Evidently, such reductions shift the mass of a given baryon's dressed-quark core into alignment with the measured Breit-Wigner mass of the associated physical states. Moreover, this pattern is seen to prevail broadly, extending to baryons in the multiplets of flavor $SU(5)$ [77,78].

Our approach thus delivers the dressed-quark-core contribution to a given observable and that this should subsequently be corrected by incorporating MB FSIs.

These features have long been appreciated and exploited in developing a successful body of work on the baryon spectrum and elastic and transition form factors, e.g., Refs. [13,34]; and we capitalize on such experience herein.

III. TRANSITION CURRENT

Electromagnetic $N \to \Delta$ transitions are described by three form factors [79]: magnetic dipole, G_M^*; electric quadrupole, G_E^*; and Coulomb (longitudinal) quadrupole, G_C^*. They arise through consideration of the transition current:

$$J_{\mu\lambda}(K,Q) = \Lambda_+(P_f) R_{\lambda\alpha}(P_f) i\gamma_5 \Gamma_{\alpha\mu}(K,Q) \Lambda_+(P_i), \tag{6}$$

where P_i and P_f are, respectively, the incoming nucleon and outgoing Δ momenta, $P_i^2 = -m_N^2$ and $P_f^2 = -m_\Delta^2$; $Q_\mu = (P_f - P_i)_\mu$ is the incoming photon momentum, $K = (P_i + P_f)/2$; and $\Lambda_+(P_i)$ and $\Lambda_+(P_f)$ are, respectively, positive-energy projection operators for the nucleon and Δ, with the Rarita-Schwinger tensor projector $R_{\lambda\alpha}(P_f)$ arising in the latter connection. (See Ref. [13], Appendix B.)

In order to succinctly express $\Gamma_{\alpha\mu}(K,Q)$, we define

$$\check{K}_\mu^\perp = \mathcal{T}^Q_{\mu\nu} \check{K}_\nu = (\delta_{\mu\nu} - \check{Q}_\mu \check{Q}_\nu) \check{K}_\nu, \tag{7}$$

with $\check{K}^2 = 1 = \check{Q}^2$, in which case

$$\Gamma_{\alpha\mu}(K,Q) = \mathfrak{k} \Bigg[\frac{\lambda_m}{2\lambda_+} (G_M^* - G_E^*) \gamma_5 \varepsilon_{\alpha\mu\gamma\delta} \check{K}_\gamma \check{Q}_\delta - G_E^* \mathcal{T}^Q_{\alpha\gamma} \mathcal{T}^K_{\gamma\mu} - \frac{i\varsigma}{\lambda_m} G_C^* \check{Q}_\alpha \check{K}_\mu^\perp \Bigg], \tag{8}$$

where $\mathfrak{k} = \sqrt{(3/2)}(1 + m_\Delta/m_N)$, $\varsigma = Q^2/[2\Sigma_{\Delta N}]$, $\lambda_\pm = \varsigma + t_\pm/[2\Sigma_{\Delta N}]$ with $t_\pm = (m_\Delta \pm m_N)^2$, $\lambda_m = \sqrt{\lambda_+ \lambda_-}$, $\Sigma_{\Delta N} = m_\Delta^2 + m_N^2$, $\Delta_{\Delta N} = m_\Delta^2 - m_N^2$.

With a concrete expression for the current in hand, one may obtain the form factors using any three sensibly chosen projection operations, e.g., with [10]

$$\mathfrak{t}_1 = \mathfrak{n} \frac{\sqrt{\varsigma(1+2\mathfrak{d})}}{\mathfrak{d} - \varsigma} \mathcal{T}^K_{\mu\nu} \check{K}_\lambda^\perp \mathrm{tr} \gamma_5 J_{\mu\lambda} \gamma_\nu, \tag{9a}$$

$$\mathfrak{t}_2 = \mathfrak{n} \frac{\lambda_+}{\lambda_m} \mathcal{T}^K_{\mu\lambda} \mathrm{tr} \gamma_5 J_{\mu\lambda}, \tag{9b}$$

$$\mathfrak{t}_3 = 3\mathfrak{n} \frac{\lambda_+}{\lambda_m} \frac{(1+2\mathfrak{d})}{\mathfrak{d} - \varsigma} \check{K}_\mu^\perp \check{K}_\lambda^\perp \mathrm{tr} \gamma_5 J_{\mu\lambda}, \tag{9c}$$

where $\mathfrak{d} = \Delta_{\Delta N}/[2\Sigma_{\Delta N}]$, $\mathfrak{n} = \sqrt{1 - 4\mathfrak{d}^2}/[4i\mathfrak{k}\lambda_m]$, and then

$$G_M^* = 3[\mathfrak{t}_2 + \mathfrak{t}_1], \qquad G_E^* = \mathfrak{t}_2 - \mathfrak{t}_1, \qquad G_C^* = \mathfrak{t}_3. \tag{10}$$

The following ratios are often considered in connection with $\gamma^* N \to \Delta$ transitions:

$$R_{\mathrm{EM}} = -\frac{G_E^*}{G_M^*}, \qquad R_{\mathrm{SM}} = -\frac{|\vec{Q}|}{2m_\Delta} \frac{G_C^*}{G_M^*} = -\frac{\Sigma_{\Delta N} \lambda_m}{2m_{\Delta^2}} \frac{G_C^*}{G_M^*}. \tag{11}$$

Since they are identically zero in $SU(6)$-symmetric constituent-quark models, they can be read as measures of deformation in one or both of the hadrons involved.

Following Refs. [13,80], the transition current in Eq. (6) can be explicated as follows:

$$J_{\mu,\alpha}(P_f,P_i) = \sum_{n=1}^{6} \int \frac{d^4p}{(2\pi)^4} \frac{d^4k}{(2\pi)^4} \times \bar{\Psi}_\alpha(-p;P_f) J_\mu^n(p,P_f,k,P_i) \Psi(k;P_i), \tag{12}$$

where Ψ_α, and Ψ are, respectively, the Δ and nucleon Faddeev amplitudes described in Sec. II and the sum ranges over the six diagrams depicted and detailed in Ref. [13], Appendix C. Each term in Eq. (12) can be evaluated using standard algebraic and numerical techniques, and results for the form factors obtained subsequently via the projections in Eqs. (9) and combinations in Eqs. (10).

In these calculations, the proton and Δ^+-baryon Faddeev amplitudes must be canonically normalized. This is achieved by computing the elastic electric form factor in each case and rescaling the amplitude such that the associated $Q^2 = 0$ value (electric charge) is unity [13]. Given this necessity, we computed the low-Q^2 behavior of all elastic form factors for each baryon and report the associated static properties of their dressed-quark cores in Table I. These results lead to the following observations:

$$r_E^{\Delta(1600)} \approx 1.4 r_E^{\Delta(1232)}, \qquad r_{M1}^{\Delta(1600)} \approx 0.95 r_{M1}^{\Delta(1232)}, \tag{13}$$

which may sensibly be compared with $r_E^{\mathrm{Roper}} \approx 1.8 r_p$ and $r_M^{\mathrm{Roper}} \approx 1.6 r_M^p$ [66]; and the octupole moments of the

TABLE I. Static properties computed from the $\Delta^+(1232)$ and $\Delta^+(1600)$ elastic form factors. An empirical value of $G_{M1}(0)$ is available for the $\Delta^+(1232)$ [4]: $3.6^{+1.3}_{-1.7} \pm 2.0 \pm 4$. Point-particle values for $J = 3/2$ states are $G_{M1}(0) = 3$, $G_{E2}(0) = -3$, $G_{M3}(0) = -1$ [81]. r_E is the root-mean-square radius computed from the baryon's $E0$ (Coulomb monopole) form factor, and all radii are listed in units of the quark-core proton charge radius, $r_p = 0.61$ fm.

Baryon	r_E	$G_{M1}(0)$	r_{M1}	$G_{E2}(0)$	r_{E2}	$G_{M3}(0)$	r_{M3}
$\Delta^+(1232)$	1.23	2.86	1.10	−6.67	1.20	−3.00	0.48
$\Delta^+(1600)$	1.68	1.50	1.05	−3.00	0.79	0.80	0.64

$\Delta(1232)$ and $\Delta(1600)$ have opposite signs, an outcome that signals the impact of differences in the distribution and strength of higher partial waves in the respective wave functions (see Fig. 2 herein and the discussion of Fig. 7 in Ref. [13]). In addition, we find that the $\Delta(1600)$ elastic electric form factor possesses a zero, at $Q^2 \approx 1.8 m_p^2$. For the $\Delta(1232)$, this zero lies at $Q^2 \approx 2.7 m_p^2$ [13]. Notably, the ordering and locations are consistent with the electric radii reported in Table I.

IV. CALCULATED FORM FACTORS: $\Delta(1232)$

Our computed $\gamma^* p \to \Delta^+(1232)$ transition form factors are depicted in Fig. 3. They are accurately interpolated using a simple functional form [82],

$$G^*_{\mathcal{F}}(x) = \frac{a_0^{\mathcal{F}} + a_1^{\mathcal{F}} x}{1 + b_1^{\mathcal{F}} x + b_2^{\mathcal{F}} x^2} \mathrm{e}^{-c_1^{\mathcal{F}} x}, \tag{14}$$

with the coefficients given in Table II. (These forms should not be used for large-x extrapolation.) We emphasize that our formulation emulates Ref. [13] in all details and the $\Delta(1232)$ results reported herein match those described in that earlier study. Hence, they serve as both a validation of the results in Ref. [13] and a benchmark against which our calculated $\gamma^* p \to \Delta^+(1600)$ transition form factors may be compared.

Considering Fig. 3, it is evident both that G_M^*, the magnetic dipole form factor, dominates this transition and our result agrees with modern data on $Q^2 \gtrsim 0.5 m_p^2$. As explained elsewhere [74,82], incorporation of MB FSIs is crucial to ensure agreement on $Q^2 \lesssim 0.5 m_p^2$; e.g., such effects increase the result by a factor of ≈ 1.5 at $Q^2 = 0$. This "meson-cloud domain" is indicated by shading in the top panel of Fig. 3. Its size typically depends on the baryon(s) being considered, e.g., extending to $Q^2 \approx 2 m_p^2$ for nucleon elastic form factors [69,84] and Roper electroproduction [31].

The $\gamma^* p \to \Delta^+(1232)$ electric and Coulomb quadrupole form factors are small but nonzero, highlighting that the dressed-quark cores of the baryons involved are deformed, viz. not purely S-wave in their rest frames. Although this is obvious from the inspection of their Poincaré-covariant wave functions (Ref. [55], Fig. 4, and Fig. 2 above), $G_{E,C}^*$ are a measurable manifestation of the distortion's magnitude. (As will subsequently become apparent, it is deformation of the Δ-baryons which is most important.)

Each panel in Fig. 3 contains three curves: the solid (black) curve is our complete prediction; the long-dashed (blue) curve is obtained when only those components of the $\Delta(1232)$ wave function are retained which correspond to S-waves in the rest frame; and the dashed (blue) curve is obtained when both the proton and $\Delta(1232)$ are reduced to S-wave states. Notably, the role played by higher partial waves in the wave functions increases with momentum

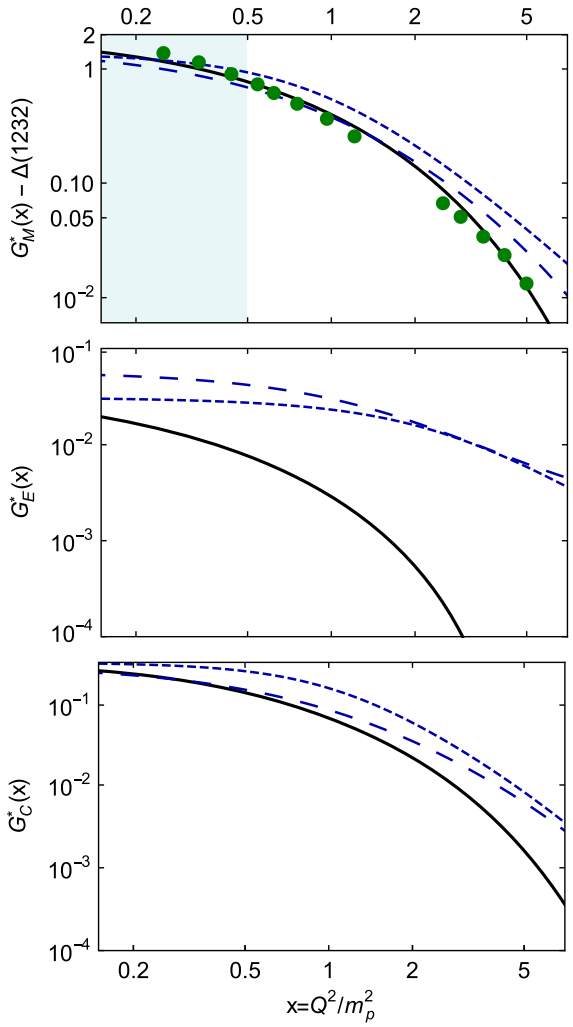

FIG. 3. *Top panel*: Magnetic dipole $\gamma^* p \to \Delta^+(1232)$ transition form factor compared with contemporary data [83]. The conventions of Ref. [79] are employed. *Middle panel*: Electric quadrupole transition form factor. *Bottom panel*: Coulomb quadrupole transition form factor. In all panels: solid (black) curve, complete result; long-dashed (blue) curve, result obtained when only those components of the $\Delta(1232)$ wave function are retained which correspond to S-waves in the rest frame; and dashed (blue) curve, obtained when both the proton and $\Delta(1232)$ are reduced to S-wave states.

TABLE II. Interpolation coefficients for each of our computed $\gamma^* p \to \Delta$ transition form factors, Eq. (14). Blank entries indicate "0".

	$\mathcal{F}$	$a_0^{\mathcal{F}}$	$a_1^{\mathcal{F}}$	$b_1^{\mathcal{F}}$	$b_2^{\mathcal{F}}$	$c_0^{\mathcal{F}}$
$\Delta(1232)$	M	1.93	4.15	3.92	3.85	0.55
	E	0.041	−0.010	4.62	0.68	0.55
	C	0.30	0.030	1.58	0.35	0.55
$\Delta(1600)$	M	0.32			0.22	0.08
	E	−0.022		−0.10	0.15	0.45
	C	0.14			0.23	0.07

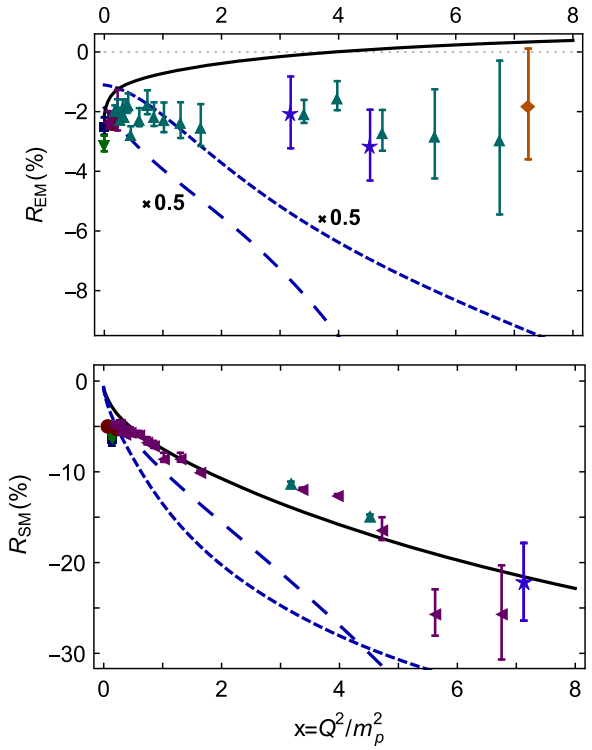

FIG. 4. $\gamma^* p \to \Delta^+(1232)$ transition, quadrupole ratios in Eq. (11): *upper panel*, $R_{\rm EM}$; and *lower panel*, $R_{\rm SM}$. In all panels: solid (black) curve, complete result; long-dashed (blue) curve, result obtained when only those components of the $\Delta(1232)$ wave function are retained which correspond to S-waves in the rest frame; and dashed (blue) curve, obtained when both the proton and $\Delta(1232)$ are reduced to S-wave states. The data in both panels are drawn from Refs. [83,86–90].

transfer (something also observed in meson form factors [85]), here generating destructive interference; agreement with data on G_M^* is impossible without the higher partial waves; and the effect of these components is very large in G_E^*, unsurprisingly, because it is a difference of two positive-definite functions. [The complete result for G_E^* exhibits a zero at $x \approx 4$, which is absent in the S-wave-only result(s).]

In Fig. 4, to further elucidate the observable impacts of higher partial waves in the Poincaré-covariant wave functions, we depict the ratios $R_{\rm EM}$ and $R_{\rm SM}$ defined in Eq. (11). The long-dashed and dashed curves in the upper panel are each multiplied by 0.5 so that they fit comfortably within the frame. The need for such multiplication highlights the substantial impact of higher partial waves on $R_{\rm EM}$. Such marked sensitivity of $R_{\rm EM}$ has been observed elsewhere [10,13,14], but the difference between our prediction for the response and that in Ref. [10] shows $R_{\rm EM}$ to be particularly susceptible to model details.

It is here worth reiterating a conclusion from Ref. [14], viz. in the $\gamma^* p \to \Delta^+(1232)$ transition, G_E^* is dominated by terms involving a scalar diquark in the proton and a pseudovector diquark in the $\Delta^+(1232)$, with photon-diquark interactions controlling the transition away from $x = 0$. It follows that, within the dressed-quark core, the electric quadrupole transition proceeds primarily by a photon transforming the 0^+-diquark in the proton into a 1^+-diquark ($\delta J = 1$) in the $\Delta^+(1232)$, with the overlap of quark-diquark components in the rest-frame Faddeev wave functions of the proton and $\Delta^+(1232)$ that differ by one unit of angular momentum. This explains why the shift induced by adding P- and D-waves in the $\Delta(1232)$ is especially large.

Given, too, that axial-vector diquark contributions interfere constructively with MB FSIs [72,73], then these features also indicate that G_E^* should be most sensitive to meson cloud contributions [13].

V. CALCULATED FORM FACTORS: $\Delta(1600)$

Predictions for the $\gamma^* p \to \Delta^+(1600)$ transition form factors are displayed in Fig. 5. Interpolations are provided by the simple functional form in Eq. (14), with the coefficients given in Table II. (Again, these forms should not be used for large-x extrapolation.) Empirical results are here only available at the real-photon point: $G_M^*(Q^2 = 0)$, $G_E^*(Q^2 = 0)$. Evidently, the quark model results—shaded grey band [91], dot-dashed (brown) curve [92], and dot-dot-dashed (orange) curve [93]—are very sensitive to the wave functions employed for the initial and final states. Furthermore, inclusion of relativistic effects has a sizable impact on transitions to positive-parity excited states [91].

Our prediction is the solid (black) curve in each panel of Fig. 5. In this instance, every transition form factor is of a unique sign on the domain displayed. Notably, the mismatches with the empirical results for $G_M^*(Q^2 = 0)$ and $G_E^*(Q^2 = 0)$ are commensurate in relative sizes with those in the $\Delta(1232)$ case, suggesting that MB FSIs are of similar importance in both channels.

As remarked above, axial-vector diquark contributions interfere constructively with MB FSIs; hence, regarding form factors, one can mimic some effects of a meson cloud by modifying the axial-vector diquark content of the participating hadrons. Accordingly, to illustrate the potential impact of MB FSIs, we computed the transition form factors using an enhanced axial-vector diquark content in the proton. This was achieved by setting $m_{1^+} = m_{0^+} = 0.85$ GeV, values with which the proton's mass is practically unchanged. The procedure produced the dotted (green) curves in Fig. 5; better aligning the $x \simeq 0$ results with experiment and suggesting thereby that MB FSIs will improve our predictions.

The short-dashed (blue) curve in Fig. 5 is the result obtained when only rest-frame S-wave components are retained in the wave functions of the proton and $\Delta(1600)$-baryon; the long-dashed (blue) curve is that computed with

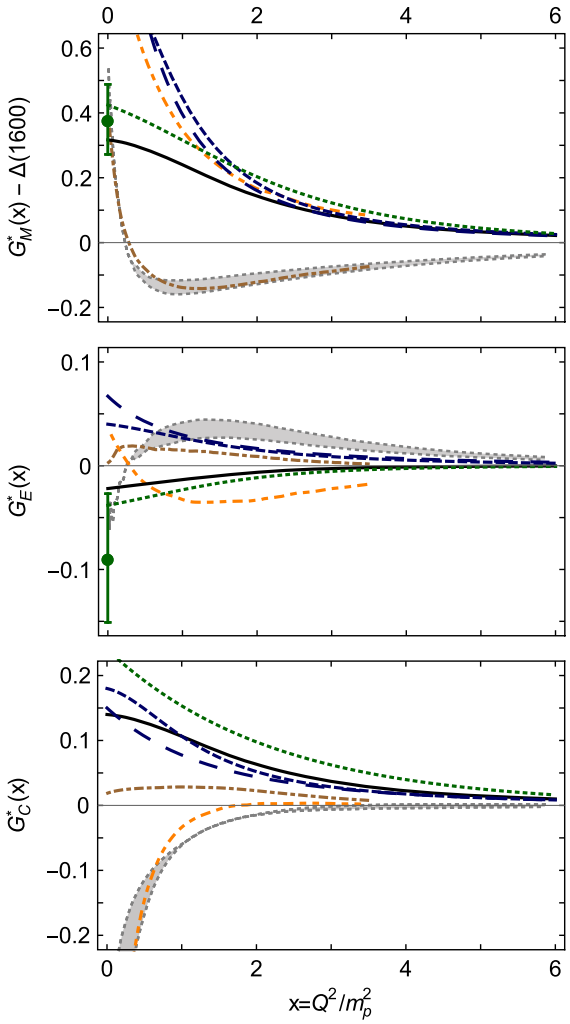

FIG. 5. *Top panel*: Magnetic dipole $\gamma^* p \to \Delta^+(1600)$ transition form factor; *middle*: electric quadrupole; and *bottom*: Coulomb quadrupole. Data from Ref. [4] and the conventions of Ref. [79] are employed. All panels: solid (black) curve, complete result; long-dashed (blue) curve, result obtained when $\Delta(1600)$ is reduced to S-wave state; dashed (blue) curve, both the proton and $\Delta(1600)$ are reduced to S-wave states; dotted (green) curve, obtained by enhancing proton's axial-vector diquark content; shaded (grey) band, light-front relativistic Hamiltonian dynamics (LFRHD) [91]; dot-dashed (brown) curve, light-front relativistic quark model (LFRQM) with unmixed wave functions [92]; and dot-dot-dashed (orange) curve, LFRQM with configuration mixing [93].

a complete proton wave function and a S-wave-projected $\Delta(1600)$. Once again, the higher partial waves have a visible impact on all form factors, with G_E^* being most affected: the higher waves produce a change in sign. This reemphasizes one of the conclusions from the quark model studies, viz. data on the $\gamma^* p \to \Delta^+(1600)$ transition form factors will be sensitive to the structure of the $\Delta^+(1600)$.

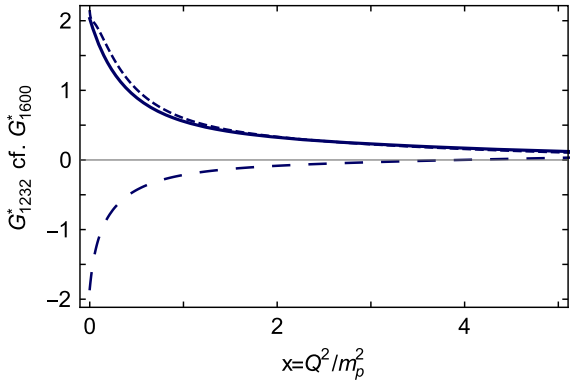

FIG. 6. Comparison between transition form factors via the following ratios: solid curve, $\frac{1}{3}G^*_{M1232}/G^*_{M1600}$; long-dashed curve, G^*_{E1232}/G^*_{E1600}; short-dashed curve, G^*_{C1232}/G^*_{C1600}.

A direct comparison between the $\gamma^* p \to \Delta^+(1232)$ and $\gamma^* p \to \Delta^+(1600)$ transition form factors is presented in Fig. 6. In all cases, the $\Delta(1232)$ form factors are larger in magnitude at small x. However, with increasing x, there is always a point at which the ordering is reversed: $x \approx 2$ for G_M^*; $x \approx 0.5$ for G_E^*; and $x \approx 1$ for G_C^*. These observations indicate that the dressed-quark-core component of the $\gamma^* p \to \Delta^+(1600)$ transition is more localized in configuration space, i.e., more pointlike, than that of the $\gamma^* p \to \Delta^+(1232)$ transition. In fact, using the dominant transition form factor, G_M^*, as a guide, the $\Delta^+(1600)$ transition radius is $\approx 1/3$ that of the $\Delta^+(1232)$.

Considering $\gamma^* p \to \Delta^+(1232)$, helicity conservation arguments within pQCD have been used to make the following predictions for the ratios in Eq. (11) [8]:

$$R_{\rm EM} \overset{Q^2\to\infty}{=} 1, \qquad R_{\rm SM} \overset{Q^2\to\infty}{=} \text{constant}, \tag{15}$$

up to $\ln^2 Q^2$ corrections [94]. These predictions disagree markedly with the outcomes produced by $SU(6)$-based quark models: $R_{\rm EM} \equiv 0 \equiv R_{\rm SM}$; and they are inconsistent with available data [5,6]. Notwithstanding such contradictions, Eqs. (15) are indubitably correct, but evidence for an approach to these limits will probably not become apparent until $x \gtrsim 20$ [12].

Our predictions for the ratios in Eqs. (11) associated with the $\gamma^* p \to \Delta^+(1600)$ transition are depicted in Fig. 7. The reasoning in Ref. [8] should equally apply to this case; hence, Eqs. (15) will become evident at some (very) large value of x. At accessible scales, however, as we have repeatedly highlighted, dynamical features of the bound-state wave functions control the x-dependence of these ratios. Examining Fig. 7, one sees that $R_{\rm EM}$ for the $\Delta(1600)$ transition is far larger in magnitude than the analogous result for the $\Delta(1232)$ final state (and opposite in sign). This is an observable manifestation of the enhanced D-wave strength in the

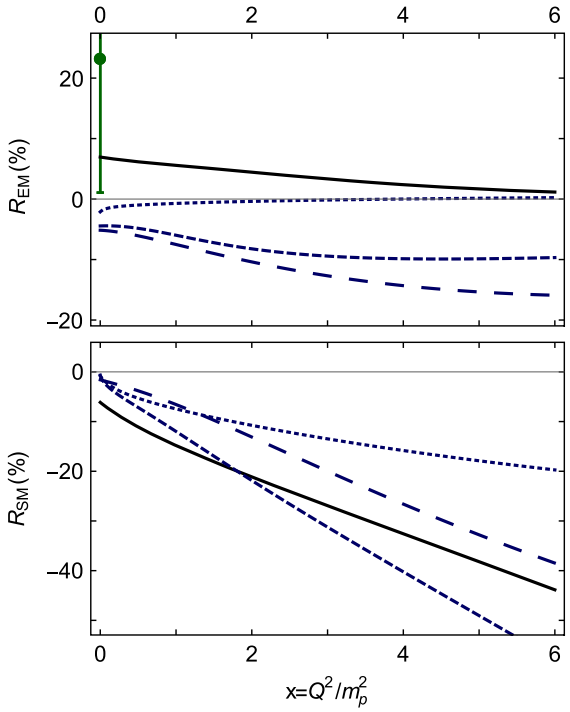

FIG. 7. *Top panel*: R_{EM}. Solid (black) curve, our prediction for the $\gamma^* p \to \Delta^+(1600)$ transition; long-dashed (blue) curve, result obtained when $\Delta(1600)$ is reduced to S-wave state; dashed (blue) curve, obtained when both the proton and $\Delta(1600)$ are reduced to S-wave states; dotted (blue) curve, this ratio for $\gamma^* p \to \Delta^+(1232)$ transition. *Bottom panel*: R_{SM}. Legend as in the upper panel.

$\Delta(1600)$ relative to that in the $\Delta(1232)$, which is apparent in Fig. 2.

VI. FORM FACTOR DISSECTIONS: $\Delta(1600)$

In connection with Eq. (12), we noted that the vertex sufficient to express the interaction of a photon with a baryon generated by the Faddeev equation in Fig. 1 is a sum of six terms, with the photon separately probing the quarks and diquarks in various ways. Hence, diverse features of quark dressing and the quark-quark correlations all play a role in determining the form factors. To elaborate, electroproduction form factors involving the nucleon and its excitations may be dissected in two separate ways, each of which can be considered as a sum of three distinct terms [14]:

DD = diquark dissection

[*DD1*] scalar diquark, $[ud]$, in both the initial- and final-state baryons,

[*DD2*] pseudovector diquark in both the initial and final states (Δ^+: $\{uu\}$ or $\{ud\}$), and

[*DD3*] a different diquark in the initial and final states.

DS = scatterer dissection

[*DS1*] photon strikes a bystander dressed quark, with the accompanying diquark untouched (Diagram 1 in Ref. [13], Fig. C.1);

[*DS2*] photon interacts with a diquark, elastically or causing a transition scalar $\leftrightarrow$ pseudovector while the accompanying bystander quark is unaffected (Diagrams 2 and 4 in Ref. [13], Fig. C.1); and

[*DS3*] photon strikes a dressed-quark in-flight, as one diquark breaks up and another is formed (Diagram 3 in Ref. [13], Fig. C.1), or appears in one of the two associated "seagull" terms (Diagrams 5 and 6).

The anatomy of a given transition is revealed by merging the information provided by DD and DS. With a Δ-baryon in the final state, *DD1* does not contribute because the $I = 0$ diquark plays no role in an $I = 3/2$ baryon.

The structure of G_M^* in the $\gamma^* p \to \Delta(1600)$ transition is revealed in the upper row of Fig. 8. The left panel shows that *DD2* is far stronger than *DD3*, and the right panel reveals that *DS1* is overwhelmingly dominant, viz. the largest contribution to G_M^* is provided by diagrams in which a photon scatters from the bystander quark, flipping its spin, in the presence of an idle pseudovector diquark. This is similar to the nature of G_M^* in the $\gamma^* p \to \Delta(1232)$ transition [14], although the 0^+-to-1^+ diquark transition component is a much smaller fraction for the $\Delta(1600)$ final state. One should also recall Fig. 6, which depicts the x-dependence of the relative magnitudes of G_M^* for the two final states.

The electric quadrupole transition form factor, G_E^*, for the $\Delta(1600)$ final state is dissected in the middle row of Fig. 8. The left panel shows that *DD2* and *DD3* are of comparable size, and the right panel that *DS1* is dominant, with *DS2* and *DS3* approximately canceling. Hence, the transition is dominated by diagrams in which the photon scatters from the bystander quark, leaving its spin unchanged, with the strength of the transition resulting from the overlap between what may be said to be quark-diquark components in the rest-frame Faddeev wave functions of the proton and $\Delta^+(1600)$ that differ by two units of angular momentum. This is markedly different from G_E^* in the $\Delta(1232)$ transition, described in connection with Fig. 5.

The anatomy of G_C^* is revealed in the bottom row of Fig. 8. Evidently, the behavior is largely determined by *DD2* and *DS1* processes, i.e., the transition strength and x-dependence measure the overlap between S- and D-wave quark-diquark angular momentum components in the rest-frame proton and $\Delta^+(1600)$ Faddeev wave functions. The marked impact of the proton's D-wave component on the full result is highlighted by the lower panel of Fig. 7. Much the same observations are true in the $\gamma^* p \to \Delta(1232)$ transition [14].

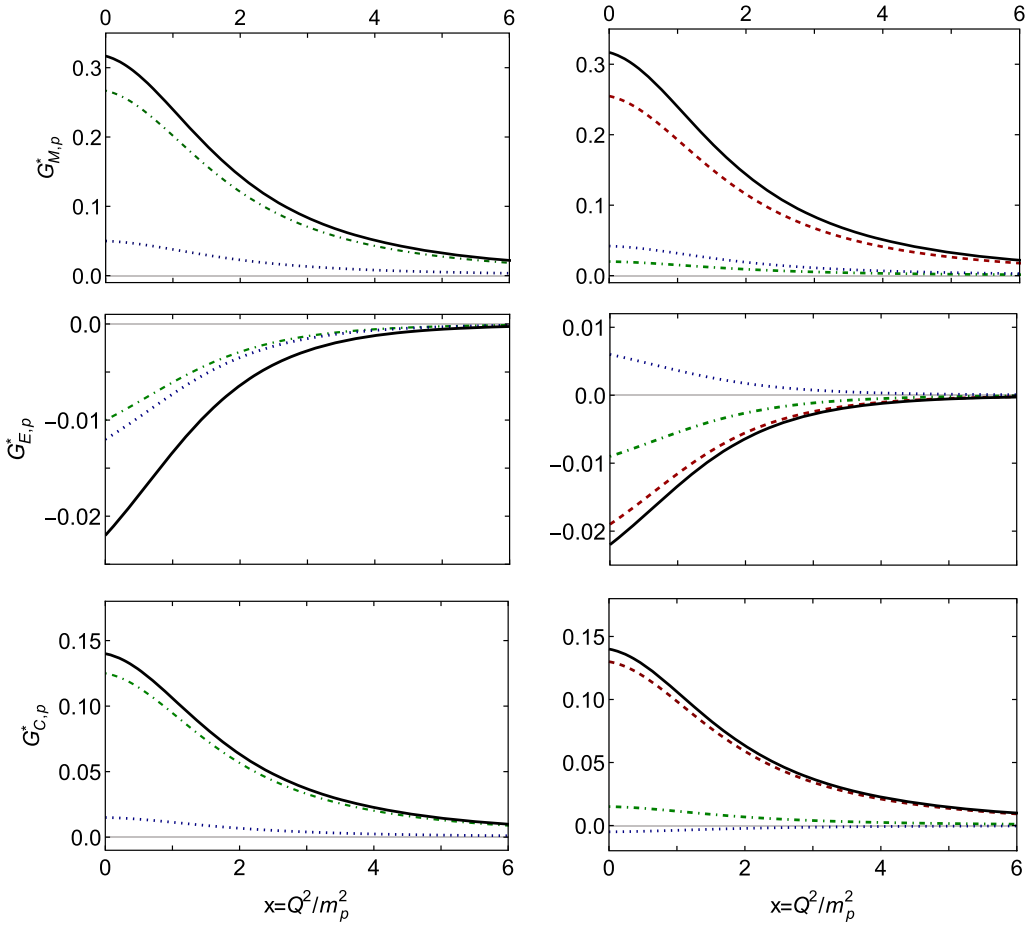

FIG. 8. $\gamma^* p \to \Delta^+(1600)$ transition form factors. *Left panels*: Diquark breakdown: *DD2* (dot-dashed green curve), pseudovector diquark in both initial and final states; *DD3* (dotted blue curve), scalar diquark in incoming baryon, pseudovector diquark in outgoing baryon. *Right panels*: Scatterer breakdown: *DS1* (red dashed curve), photon strikes an uncorrelated dressed quark; *DS2* (dot-dashed green curve), photon strikes a diquark; and *DS3* (dotted blue curve), diquark breakup contributions, including photon striking exchanged dressed-quark.

VII. SUMMARY AND PERSPECTIVES

We computed $\gamma^* p \to \Delta^+(1232)$, $\Delta^+(1600)$ transition form factors using a quark-diquark approximation to the Poincaré-covariant three-body bound-state problem in relativistic quantum field theory, unifying their treatment with that of nucleon elastic form factors [13] and $\gamma^* N \to R$ transitions [57,66]. Crucially, the diquark correlations are nonpointlike and fully dynamical, and the Faddeev kernel ensures that every valence-quark participates actively in all diquark correlations to the fullest extent allowed by kinematics and symmetries. Moreover, each dressed-quark is characterized by a nonperturbatively generated running mass function, expressing a signature consequence of dynamical chiral symmetry breaking in the Standard Model [95,96]. The $\Delta(1600)$-baryon generated by this approach is the simplest radial excitation of the $\Delta(1232)$ (Sec. II, Fig. 2); viz. it is analogous to the Roper resonance in the nucleon sector [31].

Regarding the $\gamma^* p \to \Delta^+(1232)$ transition, precise measurements already exist on $0 \leq Q^2 \lesssim 8$ GeV^2 [5,6]; and on $Q^2 \gtrsim 0.5 m_p^2$, i.e., outside the meson cloud domain for this process, our calculated magnetic dipole and Coulomb quadrupole form factors agree well with these data (Sec. IV, Figs. 3 and 4). Consistent with the data, too, we find that the electric quadrupole form factor is very small in magnitude; hence, it is particularly sensitive to the diquark content and quark-diquark angular-momentum structure of the baryons involved, and also to MB FSIs on a larger domain than the other form factors.

Our predictions for the $\gamma^* p \to \Delta^+(1600)$ magnetic dipole and electric quadrupole transition form factors are consistent with the empirical values at the real photon point, but we expect inclusion of meson-baryon final-state interactions to improve the agreement on $Q^2 \simeq 0$ (Sec. V, Fig. 5). On the other hand, the predictions extend to $Q^2 \approx 6 m_p^2$, i.e., beyond the meson-cloud domain; hence,

a meaningful direct comparison with existing data [32,33] will be possible once the analysis is completed.

It is interesting to observe that while all $\gamma^* p \to \Delta^+(1232)$ transition form factors are larger in magnitude than those for $\gamma^* p \to \Delta^+(1600)$ in some neighborhood of $Q^2 = 0$, this ordering is reversed on $Q^2 \gtrsim 2m_p^2$ (Sec. V, Fig. 6). One can thus argue that the $\gamma^* p \to \Delta^+(1600)$ transition is more localized in configuration space.

It is also notable that $R_{\rm SM}$ is qualitatively similar for both transitions considered herein; but $R_{\rm EM}$ is markedly different, being of opposite sign on $Q^2 \lesssim 4m_p^2$ and uniformly larger in magnitude for the $\Delta(1600)$ (Sec. V, Fig. 7). These observations again highlight the sensitivity of the electric quadrupole form factor to the degree of deformation of the Δ-baryons. Diquark and scatterer dissections of the transition form factors were useful in developing an understanding of the key reaction mechanisms for each electroproduction form factor (Sec. VI).

There are numerous worthwhile extensions of our analysis; e.g., calculation of the $\gamma^* p \to N(1535)1/2^-$ transition form factors is already underway. Here the final state is the nucleon's parity partner, which holds a special place in QCD owing to the manifest role of DCSB in generating the mass splitting between this state and the nucleon. The $N(1535)1/2^-$ wave function is qualitatively different from that of the near-lying Roper resonance [55]: the pointwise behavior of each component is simpler, but there are more components because pseudoscalar and vector diquark correlations are also present in this negative-parity bound state. Consequently, analyses of $\gamma^* p \to N(1535)1/2^-$ explore novel aspects of baryon structure. For instance, as $\gamma^* p \to \Delta$ transitions are sensitive to the relative strength of scalar and axial-vector diquarks within the proton (Sec. VI), then one should expect $\gamma^* p \to N(1535)1/2^-$ to reveal the relative strength of positive and negative parity diquarks in the $N(1535)1/2^-$ because negative-parity diquarks are negligible in the proton. It should be possible to test related predictions on the domain $Q^2 \gtrsim 2m_p^2$ because data already exist on $0 \leq Q^2 \lesssim 6m_p^2$ [5,6]. Moreover, given the relative ease of separating low-lying states of opposite parity, lattice-regularized QCD may also be able to contribute [97].

An analogue of $\gamma^* p \to N(1535)1/2^-$ is $\gamma^* p \to \Delta(1700)3/2^-$, in which the final state is the Δ-baryon's parity partner. Comparison between the electroproduction form factors for this process and those calculated herein would provide additional insights into the role played by DCSB in hadron structure.

Computation of $\gamma^* p \to N(1710)1/2^+$ electroproduction form factors is also valuable because the structure of the $N(1710)1/2^+$ is unclear. In quark models, the profile of its wave function is sensitive to the formulation. For instance, it can be Roper-like, with two peaks skewed relative to those in the kindred Roper wave function [98,99], in which case it may be a candidate for the system which is predominantly quark-plus-radially excited diquark; or it can have three peaks, located on the same trajectory as the two in the related Roper wave function [16,100], viz. the second radial excitation of the quark-plus-diquark system. A third possibility, realized in some dynamical coupled channels calculations [76], sees the Roper and $N(1710)1/2^+$ as both derived from the same quark core state. Given that $N(1710)1/2^+$ electroproduction data exist on $Q^2 \lesssim 4m_p^2$ [101] and that each helicity amplitude appears to be of a unique sign, unlike those for the Roper [83,102,103], it is worth testing these possibilities by exploring the solution space of the Poincaré-covariant Faddeev equation and using the results to compute the transition form factors.

As a final class of examples, we note that a complement to the analyses highlighted above is offered by studies of electroproduction form factors for low-lying baryons with "mixed" spin-isospin structure, viz. $(I, J) = (1/2, 3/2^\pm)$, $(3/2, 1/2^\pm)$. For such systems, the normal level ordering has negative-parity states lighter than positive-parity states: DCSB must still generate the (large) splitting from the ground-state baryon, but the connection with parity is reversed. Data on the $N(1520)3/2^-$ electrocouplings are available to $Q^2 \lesssim 4m_p^2$ [83,102–104]. Based upon this, some coupled-channels studies indicate that MB FSIs are (almost) negligible for the $A_{1/2}$ helicity amplitude [7,75], the calculation of which might therefore serve as a good test of the dressed-quark-core approach exploited herein.

ACKNOWLEDGMENTS

We are grateful for constructive comments from L. Chang, R. Gothe, V. Mokeev, K. Raya, F. Wang, and S.-S. Xu; for the hospitality and support of RWTH Aachen University, III. Physikalisches Institut B, Aachen—Germany; and likewise for the hospitality and support of the University of Huelva, Huelva—Spain, and the University of Pablo de Olavide, Seville—Spain, during the "4th Workshop on Nonperturbative QCD" (University of Pablo de Olavide). This work is supported by National Natural Science Foundation of China, Grants No. 11535005, No. 11690030, No. 11805097; Jiangsu Province Natural Science Foundation Grant No. BK20180323; Jiangsu Province *Hundred Talents Plan for Professionals*; Fundaćão de Amparo à Pesquisa do Estado de São Paulo—FAPESP Grant No. 2015/21550-4; U.S. Department of Energy, Office of Science, Office of Nuclear Physics, under Contract No. DE-AC02-06CH11357; Forschungszentrum Jülich GmbH; and Ministerio de Economia Industria y Competitividad (MINECO), under Grant No. FPA2017-86380-P.

[1] E. Fermi, H. Anderson, A. Lundby, D. Nagle, and G. Yodh, Phys. Rev. **85**, 935 (1952).
[2] H. Anderson, E. Fermi, E. Long, and D. Nagle, Phys. Rev. **85**, 936 (1952).
[3] D. E. Nagle, The Delta: The first pion nucleon resonance, its discovery and applications, Los Alamos National Laboratory Report No. LALP-84-27, 1984.
[4] M. Tanabashi *et al.* (Particle Data Group), Phys. Rev. D **98**, 030001 (2018).
[5] I. Aznauryan, V. Burkert, T.-S. Lee, and V. Mokeev, J. Phys. Conf. Ser. **299**, 012008 (2011).
[6] I. Aznauryan and V. Burkert, Prog. Part. Nucl. Phys. **67**, 1 (2012).
[7] I. Aznauryan *et al.*, Int. J. Mod. Phys. E **22**, 1330015 (2013).
[8] C. E. Carlson, Phys. Rev. D **34**, 2704 (1986).
[9] V. Pascalutsa, M. Vanderhaeghen, and S. N. Yang, Phys. Rep. **437**, 125 (2007).
[10] G. Eichmann and D. Nicmorus, Phys. Rev. D **85**, 093004 (2012).
[11] J. Segovia, C. Chen, C. D. Roberts, and S.-L. Wan, Phys. Rev. C **88**, 032201(R) (2013).
[12] J. Segovia, C. Chen, I. C. Cloët, C. D. Roberts, S. M. Schmidt, and S. Wan, Few-Body Syst. **55**, 1 (2014).
[13] J. Segovia, I. C. Cloët, C. D. Roberts, and S. M. Schmidt, Few-Body Syst. **55**, 1185 (2014).
[14] J. Segovia and C. D. Roberts, Phys. Rev. C **94**, 042201(R) (2016).
[15] C. Alexandrou, C. Papanicolas, and M. Vanderhaeghen, Rev. Mod. Phys. **84**, 1231 (2012).
[16] E. Santopinto and M. M. Giannini, Phys. Rev. C **86**, 065202 (2012).
[17] H. Sanchis-Alepuz, R. Alkofer, and C. S. Fischer, Eur. Phys. J. A **54**, 41 (2018).
[18] A. J. Buchmann, Few-Body Syst. **59**, 145 (2018).
[19] C. D. Roberts, J. Phys. Conf. Ser. **630**, 012051 (2015).
[20] V. D. Burkert, Few-Body Syst. **59**, 57 (2018).
[21] C. D. Roberts, Few-Body Syst. **59**, 72 (2018).
[22] L. D. Roper, Phys. Rev. Lett. **12**, 340 (1964).
[23] P. Bareyre *et al.*, C. Bricman, G. Valladas, G. Villet, J. Bizard, and J. Seguinot, Phys. Lett. **8**, 137 (1964).
[24] P. Auvil, C. Lovelace, A. Donnachie, and A. Lea, Phys. Lett. **12**, 76 (1964).
[25] S. L. Adelman, Phys. Rev. Lett. **13**, 555 (1964).
[26] L. D. Roper, R. M. Wright, and B. T. Feld, Phys. Rev. **138**, B190 (1965).
[27] S. Capstick and W. Roberts, Prog. Part. Nucl. Phys. **45**, S241 (2000).
[28] V. Crede and W. Roberts, Rep. Prog. Phys. **76**, 076301 (2013).
[29] M. M. Giannini and E. Santopinto, Chin. J. Phys. **53**, 020301 (2015).
[30] B. Golli, H. Osmanović, S. Širca, and A. Švarc, Phys. Rev. C **97**, 035204 (2018).
[31] V. D. Burkert and C. D. Roberts, Rev. Mod. Phys. **91**, 011003 (2019).
[32] A. Trivedi, Few-Body Syst. **60**, 5 (2019).
[33] V. D. Burkert, V. I. Mokeev, and B. S. Ishkhanov, arXiv: 1901.09709.
[34] C. Chen, G. Krein, C. D. Roberts, S. M. Schmidt, and J. Segovia, arXiv:1901.04305.
[35] D. Binosi, L. Chang, J. Papavassiliou, and C. D. Roberts, Phys. Lett. B **742**, 183 (2015).
[36] D. Binosi, L. Chang, J. Papavassiliou, S.-X. Qin, and C. D. Roberts, Phys. Rev. D **95**, 031501(R) (2017).
[37] D. Binosi, C. Mezrag, J. Papavassiliou, C. D. Roberts, and J. Rodríguez-Quintero, Phys. Rev. D **96**, 054026 (2017).
[38] J. Rodríguez-Quintero, D. Binosi, C. Mezrag, J. Papavassiliou, and C. D. Roberts, Few-Body Syst. **59**, 121 (2018).
[39] R. T. Cahill, C. D. Roberts, and J. Praschifka, Phys. Rev. D **36**, 2804 (1987).
[40] P. Maris, Few-Body Syst. **32**, 41 (2002).
[41] P. Maris, Few-Body Syst. **35**, 117 (2004).
[42] R. T. Cahill, C. D. Roberts, and J. Praschifka, Aust. J. Phys. **42**, 129 (1989).
[43] C. J. Burden, R. T. Cahill, and J. Praschifka, Aust. J. Phys. **42**, 147 (1989).
[44] R. T. Cahill, Aust. J. Phys. **42**, 171 (1989).
[45] H. Reinhardt, Phys. Lett. B **244**, 316 (1990).
[46] G. V. Efimov, M. A. Ivanov, and V. E. Lyubovitskij, Z. Phys. C **47**, 583 (1990).
[47] G. Eichmann, R. Alkofer, A. Krassnigg, and D. Nicmorus, Phys. Rev. Lett. **104**, 201601 (2010).
[48] G. Cates, C. de Jager, S. Riordan, and B. Wojtsekhowski, Phys. Rev. Lett. **106**, 252003 (2011).
[49] C. D. Roberts, R. J. Holt, and S. M. Schmidt, Phys. Lett. B **727**, 249 (2013).
[50] J. Segovia, C. D. Roberts, and S. M. Schmidt, Phys. Lett. B **750**, 100 (2015).
[51] G. Eichmann, Few-Body Syst. **57**, 965 (2016).
[52] G. Eichmann, C. S. Fischer, and H. Sanchis-Alepuz, Phys. Rev. D **94**, 094033 (2016).
[53] G. Eichmann, Few-Body Syst. **58**, 81 (2017).
[54] Y. Lu, C. Chen, C. D. Roberts, J. Segovia, S.-S. Xu, and H.-S. Zong, Phys. Rev. C **96**, 015208 (2017).
[55] C. Chen, B. El-Bennich, C. D. Roberts, S. M. Schmidt, J. Segovia, and S. Wan, Phys. Rev. D **97**, 034016 (2018).
[56] C. Mezrag, J. Segovia, L. Chang, and C. D. Roberts, Phys. Lett. B **783**, 263 (2018).
[57] C. Chen, Y. Lu, D. Binosi, C. D. Roberts, J. Rodríguez-Quintero, and J. Segovia, Phys. Rev. D **99**, 034013 (2019).
[58] M. Anselmino, E. Predazzi, S. Ekelin, S. Fredriksson, and D. B. Lichtenberg, Rev. Mod. Phys. **65**, 1199 (1993).
[59] R. G. Edwards, J. J. Dudek, D. G. Richards, and S. J. Wallace, Phys. Rev. D **84**, 074508 (2011).
[60] C. D. Roberts, J. Phys. Conf. Ser. **706**, 022003 (2016).
[61] T. Horn and C. D. Roberts, J. Phys. G **43**, 073001 (2016).
[62] G. Eichmann, H. Sanchis-Alepuz, R. Williams, R. Alkofer, and C. S. Fischer, Prog. Part. Nucl. Phys. **91**, 1 (2016).
[63] R. B. Lehoucq, D. C. Sorensen, and C. Yang, *ARPACK Users' Guide: Solution of Large-Scale Eigenvalue Problems with Implicitly Restarted Arnoldi Methods* (Society for Industrial and Applied Mathematics, 1998).
[64] P. Maris and C. D. Roberts, Phys. Rev. C **56**, 3369 (1997).
[65] P. Maris and P. C. Tandy, Phys. Rev. C **60**, 055214 (1999).
[66] J. Segovia, B. El-Bennich, E. Rojas, I. C. Cloët, C. D. Roberts, S.-S. Xu, and H.-S. Zong, Phys. Rev. Lett. **115**, 171801 (2015).
[67] S.-X. Qin, C. D. Roberts, and S. M. Schmidt, Phys. Rev. D **97**, 114017 (2018).

[68] G. Eichmann, R. Alkofer, I. C. Cloët, A. Krassnigg, and C. D. Roberts, Phys. Rev. C **77**, 042202(R) (2008).
[69] G. Eichmann, I. C. Cloët, R. Alkofer, A. Krassnigg, and C. D. Roberts, Phys. Rev. C **79**, 012202(R) (2009).
[70] H. Kamano, Few-Body Syst. **59**, 24 (2018).
[71] M. Döring, Few-Body Syst. **59**, 140 (2018).
[72] N. Ishii, Phys. Lett. B **431**, 1 (1998).
[73] M. B. Hecht, C. D. Roberts, M. Oettel, A. W. Thomas, S. M. Schmidt, and P. C. Tandy, Phys. Rev. C **65**, 055204 (2002).
[74] B. Julia-Diaz, T. S. H. Lee, A. Matsuyama, and T. Sato, Phys. Rev. C **76**, 065201 (2007).
[75] B. Julia-Diaz, T. S. H. Lee, A. Matsuyama, T. Sato, and L. C. Smith, Phys. Rev. C **77**, 045205 (2008).
[76] N. Suzuki, B. Juliá-Díaz, H. Kamano, T.-S. H. Lee, A. Matsuyama, and T. Sato, Phys. Rev. Lett. **104**, 042302 (2010).
[77] S.-x. Qin, C. D. Roberts, and S. M. Schmidt, Few-Body Syst. **60**, 26 (2019).
[78] P.-L. Yin *et al.*, arXiv:1903.00160.
[79] H. F. Jones and M. D. Scadron, Ann. Phys. (N.Y.) **81**, 1 (1973).
[80] M. Oettel, M. Pichowsky, and L. von Smekal, Eur. Phys. J. A **8**, 251 (2000).
[81] C. Lorce, Phys. Rev. D **79**, 113011 (2009).
[82] T. Sato and T. S. H. Lee, Phys. Rev. C **63**, 055201 (2001).
[83] I. Aznauryan *et al.*, Phys. Rev. C **80**, 055203 (2009).
[84] G. Eichmann, Phys. Rev. D **84**, 014014 (2011).
[85] P. Maris and C. D. Roberts, Phys. Rev. C **58**, 3659 (1998).
[86] R. Beck *et al.*, Phys. Rev. C **61**, 035204 (2000).
[87] T. Pospischil *et al.*, Phys. Rev. Lett. **86**, 2959 (2001).
[88] G. Blanpied *et al.*, Phys. Rev. C **64**, 025203 (2001).
[89] N. Sparveris *et al.*, Phys. Rev. Lett. **94**, 022003 (2005).
[90] S. Stave *et al.*, Phys. Rev. C **78**, 025209 (2008).
[91] S. Capstick and B. D. Keister, Phys. Rev. D **51**, 3598 (1995).
[92] I. G. Aznauryan and V. D. Burkert, Phys. Rev. C **92**, 035211 (2015).
[93] I. G. Aznauryan and V. D. Burkert, arXiv:1603.06692.
[94] A. Idilbi, X.-d. Ji, and J.-P. Ma, Phys. Rev. D **69**, 014006 (2004).
[95] National Research Council, *Nuclear Physics: Exploring the Heart of Matter* (National Academies Press, Washington, DC, 2013).
[96] S. J. Brodsky *et al.*, arXiv:1502.05728.
[97] V. Braun *et al.*, Phys. Rev. Lett. **103**, 072001 (2009).
[98] S. Capstick, Phys. Rev. D **46**, 1965 (1992).
[99] T. Melde, W. Plessas, and B. Sengl, Phys. Rev. D **77**, 114002 (2008).
[100] G. F. de Teramond, H. G. Dosch, and S. J. Brodsky, Phys. Rev. D **91**, 045040 (2015).
[101] K. Park *et al.*, Phys. Rev. C **91**, 045203 (2015).
[102] V. I. Mokeev *et al.*, Phys. Rev. C **86**, 035203 (2012).
[103] V. I. Mokeev *et al.*, Phys. Rev. C **93**, 025206 (2016).
[104] M. Dugger *et al.*, Phys. Rev. C **79**, 065206 (2009).